23. K. Yamamoto, H. Ichijo, S. J. Korsmeyer, *Mol. Cell. Biol.* **19**, 8469 (1999); R. K. Srivastava *et al.*, *Proc. Natl. Acad. Sci. U.S.A.* **96**, 3775 (1999); K. Maundrell *et al.*, *J. Biol. Chem.* **272**, 25238 (1997); S. Haldar, N. Jena, C. M. Croce, *Proc. Natl. Acad. Sci. U.S.A.* **92**, 4507 (1995).
24. X. M. Yin *et al.*, *Nature* **400**, 886 (1999); H. Li, H. Zhu, C. J. Xu, J. Yuan, *Cell* **94**, 491 (1998); X. Luo *et al.*, *Cell* **94**, 481 (1998).
24. E. Bossy-Wetzel, D. D. Newmeyer, D. R. Green, *EMBO J.* **17**, 37 (1998).
25. MEF were prepared from day 13.5 embryos and cultured in Dulbecco's modified Eagle's medium supplemented with 10% fetal bovine serum (Life Technologies). All experiments were done with cells between passage 2 and passage 5. Similar data were obtained in experiments with independently isolated MEF.
26. Frozen cell pellets were lysed on ice (30 min) in RIPA buffer [50 mM tris-HCl (pH 7.5), 10 mM β-glycerophosphate, 5 mM EDTA, 150 mM NaCl, 1% Nonidet P-40, 1 mM phenylmethylsulfonyl fluoride, 1 mM sodium orthovanadate, aprotinin at 0.4 unit/ml, and leupeptin at 0.4 unit/ml]. Extracts (100 μg of protein) were examined by protein immunoblot analysis by probing with antibodies to PKB/AKT (New England Biolabs), p38 MAPK (Santa Cruz), ERK (Santa Cruz), JNK (Pharmingen), MKK4 (Santa Cruz), MKK7 (Zymed), p53 (Calbiochem), p73 (provided by W. G. Kaelin Jr.), ARF (Novus Biologicals), caspase 3 (Santa Cruz), active caspase 3 [A. Srinivasan *et al.*, *Cell Death Differ.* **5**, 1004 (1998)], p21 (Santa Cruz), Bcl2 (Pharmingen), Bax (Pharmingen), and actin (Calbiochem). S100 fractions were prepared [J. Yang *et al.*, *Science* **275**, 1129 (1997)] and examined by immunoblot analysis by probing with antibodies to cytochrome c (Pharmingen) and Bid (provided by X. Wang). Immune complexes were detected by enhanced chemiluminescence (Kirkegaard & Perry).
27. MAPK activity was measured by in vitro kinase assays [J. Raingeaud *et al.*, *J. Biol. Chem.* **270**, 7420 (1995)]. Apoptosis was examined by analysis of DNA fragmentation by the cell death detection ELISA method (Boehringer Mannheim). The percentage of cells in sub-G_1 and S phase was examined by flow cytometry analysis of bromodeoxyuridine (BrdU) incorporation and propidium iodide staining [F. Dolbeare *et al.*, *Methods Cell Biol.* **33**, 207 (1990)]. The mitochondrial membrane potential was examined by loading the cells (30 min at 37°C) with 40 nM 3,3'-dihexyloxacarbocyanine iodide (Molecular Probes) and analyzing by flow cytometry [R. M. Siegel *et al.*, *J. Cell Biol.* **141**, 1243 (1998)]. Caspase 3 activity was measured by incubating the cells for 1 hour with the fluorogenic substrate PhiPhiLux-G_1D_2 (Alexis Biochemicals) and analyzing by flow cytometry [D. M. Finucane *et al.*, *J. Biol. Chem.* **274**, 2225 (1999)].
28. Cells were plated onto gridded cover slips and maintained in Dulbecco's modified Eagle's medium containing 10% fetal calf serum for 2 days before injection. Fluorescein-conjugated dextran and cytochrome c (Sigma) were dissolved in phosphate-buffered saline and microinjected into the cytoplasm. Injected cells were identified by fluorescence microscopy and apoptosis was quantified by counting the number of injected cells immediately after injection and again 2 hours after injection. Apoptotic MEF aggregate and rapidly detach from the cover slip, which makes it impossible to score for individual apoptotic cells.
29. Supported in part by a grant from the National Cancer Institute. We thank our colleagues for providing reagents essential for this study, M. Woda for assistance with fluorescence-activated cell sorter analysis, and Kathy Gemme for expert administrative assistance. R.A.F. and R.J.D. are investigators of the Howard Hughes Medical Institute.

30 November 1999; accepted 25 February 2000

Ubiquitin Protein Ligase Activity of IAPs and Their Degradation in Proteasomes in Response to Apoptotic Stimuli

Yili Yang, Shengyun Fang, Jane P. Jensen, Allan M. Weissman, Jonathan D. Ashwell*

To determine why proteasome inhibitors prevent thymocyte death, we examined whether proteasomes degrade anti-apoptotic molecules in cells induced to undergo apoptosis. The c-IAP1 and XIAP inhibitors of apoptosis were selectively lost in glucocorticoid- or etoposide-treated thymocytes in a proteasome-dependent manner before death. IAPs catalyzed their own ubiquitination in vitro, an activity requiring the RING domain. Overexpressed wild-type c-IAP1, but not a RING domain mutant, was spontaneously ubiquitinated and degraded, and stably expressed XIAP lacking the RING domain was relatively resistant to apoptosis-induced degradation and, correspondingly, more effective at preventing apoptosis than wild-type XIAP. Autoubiquitination and degradation of IAPs may be a key event in the apoptotic program.

Thymocytes undergo apoptosis in response to many stimuli, including glucocorticoids, etoposide, γ-radiation, and engagement of their receptors for antigen (*1*). Reagents that inhibit proteasomes, multicatalytic protease complexes responsible for the degradation of ubiquitinated cellular proteins (*2*), block cell death induced by many of these stimuli (*3*). One possible explanation is that proteasome-mediated degradation of anti-apoptotic proteins might be required for cell death to occur. Candidate anti-apoptotic molecules expressed in immature thymocytes include the Bcl-2 family member Bcl-x_L and members of the IAP (inhibitors of apoptosis) family (*4*). To explore this idea, we induced thymocytes to die by treating them with dexamethasone (Dex). Under these conditions, amounts of both c-IAP1 (inhibitor of apoptosis–1) and XIAP (X-linked inhibitor of apoptosis) were substantially decreased (Fig. 1A) (*5*). No change occurred in amounts of Bcl-x_L or β-actin. An increase in Dex-induced cell death was not observed until 8 hours of culture, and even at this time ~90% of thymocytes were viable (Fig. 1B). Inhibition of proteasome activity greatly reduced apoptosis at 16 hours (Fig. 1B) (*3*). Amounts of c-IAP1 and XIAP began to decrease 4 to 6 hours after culture with Dex, and by 8 hours were decreased by 64 ± 1.7% for cIAP-1 ($n = 3$) and 73 ± 3.4% for XIAP ($n = 5$) (Fig. 1D) (*6*). Etoposide is a topoisomerase II inhibitor that, unlike glucocorticoids, induces apoptosis through a p53-dependent pathway (*7*). Etoposide induced a decrease in IAP levels that was first observed after 2 to 4 hours of culture, and by 6 hours the amounts of c-IAP1 and XIAP fell ~87 ± 7.5% ($n = 3$) and 77 ± 8.5% ($n = 5$), respectively (Fig. 1E) (*6*). Cell death was first detected by trypan blue exclusion ~8 hours after addition of etoposide and was largely prevented in cells treated with proteasome inhibitors (Fig. 1C). Therefore, induction of apoptosis by two different afferent pathways resulted in relatively early and specific loss of IAPs in thymocytes.

The relatively rapid decrease in the amount of IAPs in thymocytes stimulated to undergo apoptosis raised the possibility that these proteins were being targeted for degradation. Given that the proteasome is a major effector of intracellular protein degradation and that proteasome inhibitors block glucocorticoid- and etoposide-induced thymocyte apoptosis (*3*) (Fig. 1), thymocytes were cultured with Dex or etoposide in the absence or presence of proteasome inhibitors (Fig. 2). Both a peptide aldehyde proteasome inhibitor and the highly specific proteasome inhibitor lactacystin effectively blocked the decrease in IAP expression induced by the apoptotic stimuli.

Protein ubiquitination involves the sequential action of ubiquitin activating enzyme (E1), a ubiquitin-conjugating enzyme (E2), and a ubiquitin protein ligase (E3) (*8*). Ubiquitination by some known E3's and several proteins of previously unknown function is dependent on an intact RING finger (*9*, *10*). IAPs contain a COOH-terminal RING domain, so we examined whether these molecules also have ubiq-

Laboratory of Immune Cell Biology, Division of Basic Sciences, National Cancer Institute, National Institutes of Health, Bethesda, MD 20892, USA.

*To whom correspondence should be addressed. E-mail: jda@box-j.nih.gov

uitin protein ligase activity. We used an in vitro ubiquitination assay that takes advantage of the fact that prokaryotic cells do not express the enzymes required for protein ubiquitination (*9*, *11*). Glutathione S-transferase (GST) fusion proteins with full-length XIAP (GST-XIAP), c-IAP1 (GST-cIAP1), or GST alone were added to bacterial lysates containing recombinant E1 and E2 and ^{32}P-labeled recombinant ubiquitin. After 90 min the reactions were stopped and proteins from the lysates resolved by SDS–polyacrylamide gel electrophoresis (PAGE) (Fig. 3A). In the presence of GST alone, little protein ubiquitination was detectable. In contrast, GST-XIAP and GST-cIAP1 caused a large increase in the number of ubiquitinated species. The pattern of ubiquitination for each IAP was distinct, with XIAP reproducibly yielding prominent (>180 kD) species of large molecular size and c-IAP1 generating species predominantly in the 80- to 130-kD range. We also examined GST fusions that contained a truncated form of XIAP lacking the RING domain (GST-XIAP$_{1\text{-}351}$) or XIAP or c-IAP1 in which the metal-coordinating residues His$_{467}$ or His$_{588}$ were replaced with Ala. Unlike the wild-type fusion proteins, GST-XIAP$_{1\text{-}351}$, GST-XIAP$_{H467A}$, and GST-cIAP1$_{H588A}$ did not increase the amount of ubiquitinated species in the ubiquitin protein ligase assay (Fig. 3, B and C). XIAP and c-IAP1 also mediated their own ubiquitination in vitro; in vitro–translated and metabolically labeled c-IAP1 and XIAP were ubiquitinated in an E2-dependent manner, which was increased when they were incubated with their corresponding GST fusion proteins; this activity was ablated by mutation of the RING domains (*6*).

To determine if IAPs can mediate their own ubiquitination and degradation in vivo, Myc-tagged wild-type or RING-mutated c-IAP1 were transfected into 293 cells, immunoprecipitated with antibodies to Myc (anti-Myc), and blotted with anti-Myc or anti-ubiquitin. Both IAPs were expressed (Fig. 4A), and the RING mutant was reproducibly expressed in slightly higher amounts than the wild-type protein (Fig. 4B). Wild-type c-IAP1 but not the ubiquitination-defective form was heavily ubiquitinated (Fig. 4A). This ubiquitination appears to be functionally significant, because preventing proteasome-mediated degradation with lactacystin increased the abundance of the wild-type c-IAP1 protein but caused little change in the amount of the RING mutant (Fig. 4B). Therefore, overexpressed c-IAP1 undergoes ubiquitination and degradation in cells, phenomena that do not occur (or occur to a far lesser extent) when the IAP does not have endogenous

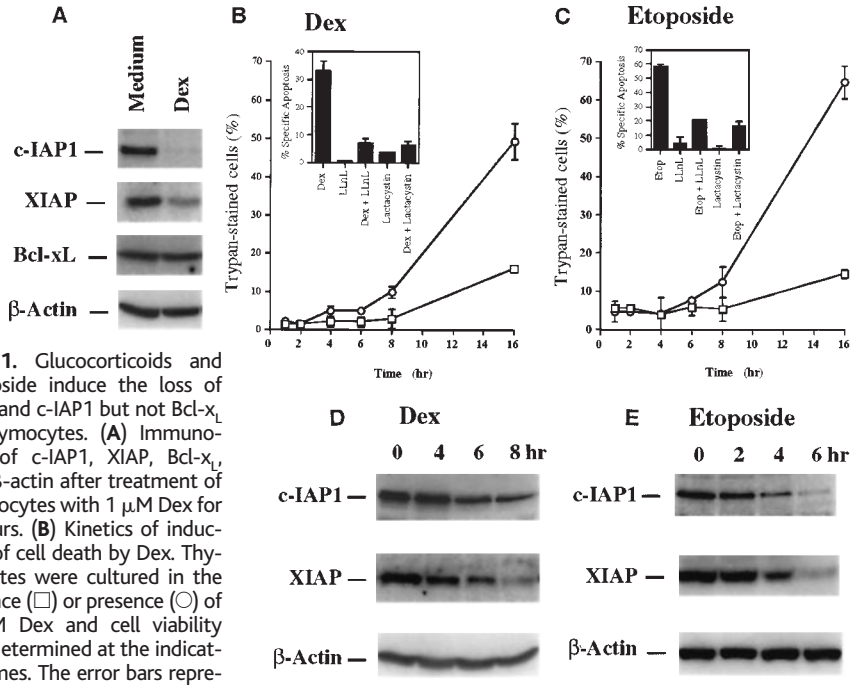

Fig. 1. Glucocorticoids and etoposide induce the loss of XIAP and c-IAP1 but not Bcl-x$_L$ in thymocytes. (**A**) Immunoblot of c-IAP1, XIAP, Bcl-x$_L$, and β-actin after treatment of thymocytes with 1 μM Dex for 8 hours. (**B**) Kinetics of induction of cell death by Dex. Thymocytes were cultured in the absence (□) or presence (○) of 1 μM Dex and cell viability was determined at the indicated times. The error bars represent the SEM of three independent experiments, each done in duplicate wells. (**Inset**) Percent specific apoptosis (±SEM) at 16 hours in the absence or presence of the proteasome inhibitors *N*-acetyl-Leu-Leu-Leu-Nle-CHO (LLnL) (50 μM) or lactacystin (50 μM) (Calbiochem, San Diego, California). Specific apoptosis is defined as the amount of apoptosis in excess of the spontaneous apoptosis of control cultures (% experimental apoptosis − % apoptosis in medium)/(100 − % apoptosis in medium). Spontaneous apoptosis ranged from 4 to 12%. (**C**) Kinetics of induction of cell death by etoposide. Thymocytes were cultured in the absence (□) or presence (○) of etoposide (10 μg/ml), and cell viability was determined at the indicated times. (**Inset**) Percent specific apoptosis (±SEM) at 16 hours in the absence or presence of the indicated proteasome inhibitors. (**D**) Immunoblot analysis of the kinetics of XIAP and c-IAP1 decreases after treatment with 1 μM Dex. (**E**) Immunoblot analysis of the kinetics of XIAP and c-IAP1 decreases after treatment with etoposide (10 μg/ml). Immunoblots were incubated with ^{125}I-labeled protein A and visualized with a Storm PhosphorImager.

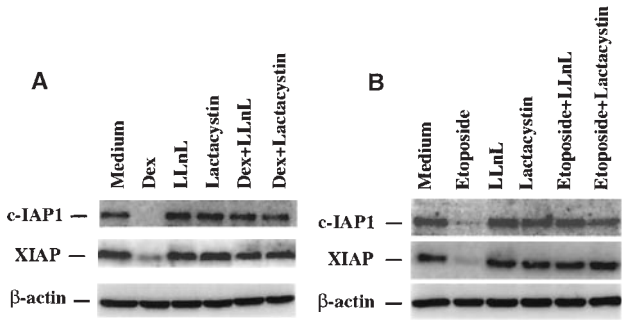

Fig. 2. Dex- and etoposide-induced decreases of XIAP and c-IAP1 can be prevented by proteasome inhibitors. (**A**) Thymocytes were cultured with 10^{-6} M Dex in the presence or absence of 50 μM LLnL or lactacystin proteasome inhibitors for 8 hours, and the levels of XIAP, c-IAP1, and β-actin were determined by immunoblot. (**B**) Thymocytes were treated with etoposide (10 μg/ml) for 6 hours in the presence or absence of 50 μM LLnL or lactacystin. The levels of XIAP, c-IAP1, and β-actin were determined by immunoblotting as in Fig. 1.

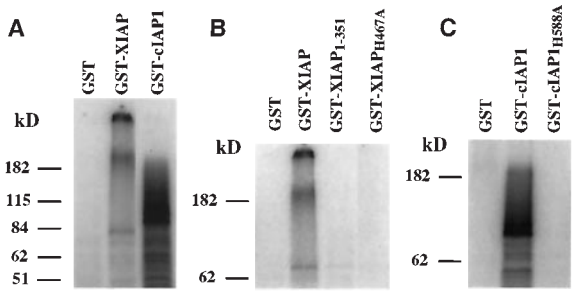

Fig. 3. (**A** to **C**) c-IAP1 and XIAP GST fusion proteins have ubiquitin protein ligase activity. The ubiquitination reaction was carried out with 2.5 pmol of bacterially expressed GST or the indicated GST fusion proteins bound to glutathione–Sepharose 4B beads added to the reaction buffer. After incubation, reaction mixtures were separated on 7.5% SDS-PAGE, and the ^{32}P-ubiquitin-labeled species were visualized with a Storm PhosphorImager.

ubiquitin protein ligase activity.

To investigate the functional relevance of the RING domain, 2B4.11 T hybridoma cells were stably transfected with full-length Flag-tagged XIAP or the RING-less $XIAP_{1-351}$ (*12*). Clones expressing equivalent amounts of the transfected gene products were chosen for further study. Treatment of untransfected 2B4.11 cells with Dex for 12 hours resulted in the loss of XIAP (Fig. 5A). As with thymocytes, amounts of β-actin did not change during this time. The amounts of transfected full-length XIAP (XFL.1 and XFL.2 cells) were also decreased after Dex treatment. In contrast, Dex caused only a small decrease in the amount of $XIAP_{1-351}$ (XT cells). Expression of tagged full-length XIAP but not truncated XIAP appeared to increase the amount of endogenous XIAP in untreated cells, as well as the relative loss of this molecule in Dex-treated cells. The maintenance of expression of the various XIAPs was correlated with resistance to apoptosis (Fig. 5B).

IAPs mediate their anti-apoptotic function, at least in part, by interactions between an ~70–amino acid NH_2-proximal domain containing three BIRs (baculovirus internal repeats) and particular caspases (*4*, *13*). The role of the COOH-terminal RING domain in inhibition of apoptosis appears to vary depending on the IAP and the cell type, its mutation or absence having either a small negative effect or a positive effect on cell survival (*14*). Although our understanding of the function of RING domains is limited, this motif appears to play a role in protein ubiquitination, and a number of RING-containing proteins have ubiquitin protein ligase activity (*9, 10*). Our results demonstrate that IAPs themselves catalyze ubiquitination in a RING-dependent manner. Moreover, these anti-apoptotic proteins are capable of autoubiquitination, and when overexpressed or expressed in cells induced to die undergo RING-dependent proteasome-mediated degradation.

Because IAPs inhibit glucocorticoid- and etoposide-induced apoptosis (*15*) (as do proteasome inhibitors), their proteasome-mediated degradation may be an important regulatory step for cells that have been signaled to undergo apoptosis to actually progress to cell death. Furthermore, the finding that IAPs can catalyze their own ubiquitination provides the interesting possibility that their abundance is actively self-regulated. This is supported by the finding that RING-less XIAP is degraded to a lesser extent, and confers better protection from apoptosis, than wild-type protein. However, the RING-less XIAP was not completely resistant to Dex-induced and proteasome-mediated degradation, indicating that this protein can also serve as a target for other E3's, perhaps endogenous XIAP or other family members. The ability of IAPs to catalyze their own ubiquitination appears to be suppressed in resting thymocytes, because proteasome inhibitors had little effect on the amount of IAP in such cells. Whether IAPs can ubiquitinate other molecules and, if so, what might be their substrates, remains to be determined.

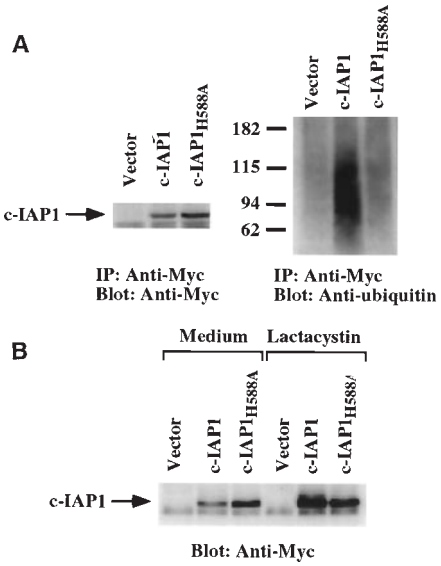

Fig. 4. The protein ubiquitin ligase activity of c-IAP1 regulates its ubiquitination and degradation in cells. The human embryonal kidney cell line 293 was transfected with the cDNA expression vector $pcDNA_3$ alone, $pcDNA_3$-myc-cIAP1, or $cDNA_3$-myc-$cIAP1_{H588A}$. (**A**) Lysate from transfected cells was immunoprecipitated with anti-Myc epitope (antibody 9E10). The antibody-coated beads were divided into two portions, and the immunoprecipitated material was immunoblotted with 9E10 or anti-ubiquitin, as indicated, and visualized with ^{125}I-labeled protein A as in Fig. 1. The transfected c-IAP1 is indicated above a minor nonspecific band. (**B**) Transfected 293 cells were treated with proteasome inhibitor lactacystin (50 μM) for 18 hours. Lysates were separated by SDS-PAGE and blotted with 9E10. Similar results were obtained in three independent experiments.

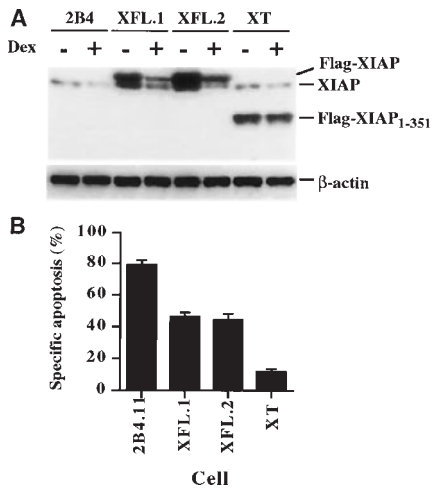

Fig. 5. Stability and efficacy of RING-less XIAP in protecting cells from glucocorticoid-induced apoptosis. 2B4.11 T hybridoma cells were stably transfected with full-length NH_2-terminal Flag-tagged XIAP or $XIAP_{1-351}$. (**A**) After treatment with 1 μM Dex for 10 hours, the indicated cells were analyzed for XIAP expression by immunoblotting with a polyclonal antibody to XIAP that recognizes both wild-type and truncated XIAP (AF822; R&D Systems, Minneapolis, MN). The blot was developed with horseradish peroxidase–labeled donkey anti-rabbit immunoglobulin G (Amersham Pharmacia Biotech, Piscataway, NJ) and SuperSignal chemiluminescent substrate (Pierce, Rockford, IL). The transfected full-length XIAP is slightly larger than the endogenous XIAP because of the Flag tag. The membrane was stripped, blotted with anti–β-actin, and developed with ^{125}I-labeled protein A. (**B**) Viability of the indicated cells was assessed by trypan blue exclusion 20 hours after treatment with 1 μM Dex. Specific cell death was calculated as in Fig. 1. The error bars are the SEM of four independent experiments, each done in duplicate wells.

References and Notes

1. J. J. Cohen *et al.*, *Annu. Rev. Immunol.* **10**, 267 (1992).
2. A. M. Weissman, *Immunol. Today* **18**, 189 (1997).
3. L. M. Grimm *et al.*, *EMBO J.* **15**, 3835 (1996).
4. S. Krajewski *et al.*, *Cancer Res.* **54**, 5501 (1994); Q. L. Deveraux *et al.*, *Nature* **388**, 300 (1997); C. S. Duckett *et al.*, *EMBO J.* **15**, 2685 (1996); S. S. Young *et al.*, *Mamm. Genome* **10**, 44 (1999).
5. For determination of cell viability, thymocytes from C57BL/6 mice were cultured at a density of 3×10^6/ml for the indicated times in medium, 1 μM Dex (Sigma, St. Louis, MO), or etoposide (10 μg/ml) (Sigma). Cell viability was determined by the exclusion of trypan blue as assessed by light microscopy. For immunoblotting, 5×10^6/ml C57BL/6 thymocytes were cultured for the indicated times in medium alone or with 1 μM Dex or etoposide (10 μg/ml). After harvesting, the cells were lysed with RIPA buffer (phosphate-buffered saline, 1% NP-40, 0.5% sodium deoxycholate, and 0.1% SDS) containing protease inhibitors AEBSF (1 mM), aprotinin (10 μg/ml), and leupeptin (10 μg/ml). Samples were separated by 10% SDS-PAGE, transferred onto nitrocellulose membranes, and blotted with primary antibodies [anti-XIAP (Transduction Laboratory, Lexington, KY), anti–Bcl-x_L (Santa Cruz Biotechnology, Santa Cruz, CA), anti–β-actin (Sigma), and anti-c-IAP1 (R & D Systems, Minneapolis, MN)]. After washing with tris-buffered saline (TBS; 10 mM tris-HCl, 150 mM NaCl, and 0.05% Tween-20), membranes were incubated with ^{125}I–protein A, washed with TBS, and visualized with a Storm PhosphorImager (Molecular Dynamics, Sunnyvale, CA).
6. Y. Yang, S. Fang, J. P. Jensen, A. M. Weissman, J. D. Ashwell, data not shown.
7. S. W. Lowe *et al.*, *Nature* **362**, 847 (1993); A. R. Clarke *et al.*, *Nature* **362**, 849 (1993).
8. A. Hershko and A. Ciechanover, *Annu. Rev. Biochem.* **67**, 425 (1998).
9. K. L. Lorick *et al.*, *Proc. Natl. Acad. Sci. U.S.A.* **96**, 11364 (1999).
10. R. J. Deshaies, *Annu. Rev. Cell Dev. Biol.* **15**, 435 (1999); K. Iwai *et al.*, *Proc. Natl. Acad. Sci. U.S.A.* **96**, 12436 (1999); J. Lisztwan *et al.*, *Genes Dev.* **13**, 1822 (1999); Y. Xie and A. Varshavsky, *EMBO J.* **18**, 6832 (1999); H. Waterman *et al.*, *J. Biol. Chem.* **274**, 22151 (1999); C. A. Joazeiro *et al.*, *Science* **286**, 309 (1999); R. Honda, H. Tanaka, H. Yasuda, *FEBS Lett.* **420**, 25 (1997); S. Fang *et al.*, *J. Biol. Chem.* **275**, 8945 (2000).
11. $XIAP_{1-315}$ was generated by polymerase chain reaction with primers (i) 5′-CGCGGATCCATGACTTTTA-

ACAGTTTTG-3′; (ii) 5′-CCCATCGATTTAACACTCC-TCAAGTGAATGAG-3′. $XIAP_{H467A}$ and $c\text{-}IAP1_{H588A}$ were made by using the QuikChange site-directed mutagenesis kit (Stratagene, La Jolla, CA) with primers (i) 5′-GTTTTTGTTCCTTGTGGAGCTCTAGTCAC-TTGTAAACAA-3′and 5′-TTGTTTACAAGTGACTA-GAGCTCCACAAGGAACAAAAAC-3′; (ii) 5′-CTGT-TGTATTTATTCCTTGTGGTGCTCTGGTAGTATGCCA-GGAATGTGC 3′ and 5′ GCACATTCCTGGCATAC-TACCAGAGCACCACAAGGAATAAATACAACAG-3′. These cDNAs were cloned into pGEX-4T-2 by using Bam H1 and Not 1 sites and confirmed by direct sequencing. The GST or GST fusion proteins were induced in DH-5α cells with 200 μM IPTG (isopropyl-β-D-thiogalactopyranoside) and purified with glutathione–Sepharose 4B. In vitro ubiquitination reactions were carried out by adding recombinant wheat E1 (20 ng), UbcH5b (20 ng), 2 μl of bacterial lysate from BL-21 cells, and ^{32}P-labeled ubiquitin (2×10^4 cpm) to the GST or GST fusion proteins in ubiquitination buffer [50 mM tris (pH 7.4), 2 mM adenosine 5′-triphosphate, 5 mM $MgCl_2$, and 2 mM dithiothreitol]. After incubating at 30°C for 90 min, the reaction mixtures were separated by 7.5% SDS-PAGE and visualized with a Storm PhosphorImager and ImageQuant software (Molecular Dynamics). After exposure, the gels were restained with Coomassie blue to ensure that similar amounts of the GST fusion proteins had been used.

12. 2B4.11 T hybridoma cells were transfected with pEBB-Flag-XIAP, pEBB-Flag-$XIAP_{H467A}$, or pEBB-Flag-$XIAP_{1\text{-}351}$ together with pCI-neo. The cells were selected with G418 (1 mg/ml) and screened with anti-Flag for expression of the transfected molecules. Two independent cell lines expressing XIAP (XFL.1 and XFL.2) and one cell line expressing $XIAP_{1\text{-}351}$ (XT) were found to have similar levels of the transfected molecules and were used for further study.
13. R. Takahashi *et al.*, *J. Biol. Chem.* **273**, 7787 (1998)
14. R. J. Clem and L. K. Miller, *Mol. Cell. Biol.* **14**, 5212 (1994); D. Vucic, W. J. Kaiser, L. K. Miller, *J. Biol. Chem.* **273**, 33915 (1998); B. A. Hay, D. A. Wassarman, G. M. Rubin, *Cell* **83**, 1253 (1995).
15. L. J. Eiben and C. S. Duckett, *Results Probl. Cell Differ.* **24**, 91 (1998).
16. We are grateful to C. Duckett (National Cancer Institute, Bethesda, MD) for providing human XIAP and c-IAP1 cDNAs and for critical review of this manuscript.

10 January 2000; accepted 20 March 2000

Seeing the Herpesvirus Capsid at 8.5 Å

Z. Hong Zhou,[1] Matthew Dougherty,[2] Joanita Jakana,[2] Jing He,[3] Frazer J. Rixon,[4] Wah Chiu[2,3]*

Human herpesviruses are large and structurally complex viruses that cause a variety of diseases. The three-dimensional structure of the herpesvirus capsid has been determined at 8.5 angstrom resolution by electron cryomicroscopy. More than 30 putative α helices were identified in the four proteins that make up the 0.2 billion–dalton shell. Some of these helices are located at domains that undergo conformational changes during capsid assembly and DNA packaging. The unique spatial arrangement of the heterotrimer at the local threefold positions accounts for the asymmetric interactions with adjacent capsid components and the unusual co-dependent folding of its subunits.

Human herpesviruses cause a variety of disorders ranging from cold sores and chicken pox to less frequent conditions, including congenital defects, blindness, and cancers as well as life-threatening complications in immunosuppressed individuals (*1*, *2*). Herpes simplex virus–type 1 (HSV-1), the prototypical member of the herpesvirus family, infects more than 60% of the United States population. The HSV-1 genome of 150,000 base pairs (bp) contains over 75 open reading frames, about half of which encode structural proteins. The herpesvirus virion is composed of a glycoprotein-containing envelope, a proteinaceous layer (tegument), and an icosahedral capsid shell of 1250 Å diameter enclosing a double-stranded DNA (dsDNA) genome (*3*). Upon entry to the cell, the external compartments disassemble, releasing the capsid, which is transported across the cytosol in association with cellular carrier proteins (*4*). At the nuclear pore, the viral DNA is released into the nucleus (*5*). New capsids are assembled around a scaffolding core inside the nucleus. Subsequently, viral DNA is packaged, possibly through a penton channel, after proteolysis and removal of scaffolding proteins (*6*).

We imaged ice-embedded HSV-1 capsids in a JEOL 4000 electron cryomicroscope with a LaB_6 gun operated at 400 kV (*7*). Despite their low contrast (Fig. 1A), the images contain data extending beyond 7 Å (Fig. 1B). By merging 5860 particle images from 130 micrographs (*8*), we determined the molecular structure to 8.5 Å resolution (Fig. 1, C through F). The validity of our structure can be gauged from several lines of evidence. These include the low-phase residuals (<45° at 8.5 Å) between two independent three-dimensional (3D) reconstructions (Fig. 1D) and the low (~58°) average-phase residual difference between raw images and computed projections from the final map up to 8.5 Å. The high degree of sixfold symmetry evident around the regions of the local sixfold symmetry axes was not enforced in the icosahedral reconstruction (Fig. 1E) and further supports the validity of the structure.

The capsid shell, with a total molecular mass of 0.2 billion daltons, is formed by four proteins whose sequences are unrelated: VP5 (149 kD), VP26 (12 kD), VP23 (34 kD), and VP19C (50 kD). An asymmetric unit has a molecular mass of ~3.2 MD and consists of 1 penton subunit, 15 hexon subunits, and 5⅓ triplexes (Fig. 1F). The major morphological units in the capsid are the pentons and the hexons, which contain five and six copies of VP5, respectively. The hexon also contains six copies of VP26, which form a ring of connected densities on top of the VP5 subunits (*9*).

Previous studies of smaller viral capsids have demonstrated that α helices can be identified at 7.4 to 9 Å resolution (*10*–*12*). At this resolution range, the mass densities of α helices have the appearance of continuous high-density rods of 5 to 7 Å diameter. We have designated a relatively high density as an α helix when it forms an extended rod of the correct diameter and is spatially resolved from neighboring densities.

In the VP5 subunit of a sixfold averaged hexon (Fig. 2A), we assigned 24 mass segments as α helices (Fig. 2B). The VP26 subunit of the hexon contains no obvious candidate helices, in agreement with its reported secondary structure (*13*). On the basis of estimates of the number of amino acids involved, the putative α helices represent ~17% of the total mass of VP5, which is of the same range as the helical content of purified VP5 estimated by far ultraviolet (UV) circular dichroism (CD) spectroscopy (*14*). Two relatively long helices (20 and 22 Å) are present in the upper domain of the VP5 subunit (Fig. 2B). A group of seven relatively short (8 to 14 Å), nearly parallel α helices is seen in the middle domain (Fig. 2, B and C). These helices are close to the narrowest constriction of the channel that runs through the center of the hexons and pentons (Fig. 1C). In pentons, this channel appears to play an important role in capsid maturation and DNA packaging (*6*). It is closed in virions, presumably to prevent the exit of the packaged DNA, but is open in purified capsids that lack DNA (*15*). The closure of the channel occurs in the region of the constriction and requires a mass

[1]Department of Pathology and Laboratory Medicine, University of Texas–Houston Medical School, Houston, TX 77030, USA. [2]National Center for Macromolecular Imaging, Department of Biochemistry and Molecular Biology, Baylor College of Medicine, Houston, TX 77030, USA. [3]Graduate Program in Structural and Computational Biology and Molecular Biophysics, Baylor College of Medicine, Houston, TX 77030, USA. [4]MRC Virology Unit, Institute of Virology, Glasgow G11 5JR, Scotland, UK.

*To whom correspondence should be addressed. E-mail: wah@bcm.tmc.edu